INTERNATIONAL JOURNAL OF ENERGY RESEARCH
Int. J. Energy Res. (2017)
Published online in Wiley Online Library (wileyonlinelibrary.com). DOI: 10.1002/er.3742

Elucidating the process of hydrogen generation from the reaction of sodium hydroxide solution and ferrosilicon

Paul Brack[1], Sandra E. Dann[1,*,†], K. G. Upul Wijayantha[1], Paul Adcock[2] and Simon Foster[2]

[1]Energy Research Laboratory, Department of Chemistry, Loughborough University, Loughborough, Leicestershire LE11 3TU, UK
[2]Intelligent Energy, Charnwood Building, Holywell Park, Ashby Road, Loughborough, Leicestershire LE11 3GB, UK

SUMMARY

For the first time, the process of hydrogen evolution from ferrosilicon 75 using sodium hydroxide solution has been investigated as a function of temperature using a combination of X-ray photoelectron spectroscopy, X-ray diffraction and physical measurements. Ferrosilicon 75, a mixture of silicon (~50 wt.%) and iron disilicide (~50 wt.%), has been shown to produce hydrogen by the action of sodium hydroxide solution on the silicon only, with the iron disilicide acting in the role of spectator/protector species for the silicon. Neither iron disilicide alone nor ferrosilicon 45, which does not contain a pure metallic silicon phase, was found to generate hydrogen under similar reaction conditions, further indicating that the presence of a pure metallic silicon phase is essential for hydrogen generation. As the iron disilicide acts as a diluent for the active silicon, it is hypothesized that this would result in a slower release of hydrogen than that which would be obtained from the reaction of silicon alone, which may be useful for applications which require a long-term, sustained release of hydrogen. A hydrogen yield of 462.5 mL/g and a maximum hydrogen generation rate of 83 mL/min g were obtained within 10 min of reaction with 40 wt.% NaOH at 348 K. © 2017 The Authors. *International Journal of Energy Research* Published by John Wiley & Sons Ltd.

KEY WORDS

chemical hydrogen storage; ferrosilicon; hydrogen generation; hydrolysis

Correspondence

*Sandra E. Dann, Department of Chemistry, Loughborough University, Loughborough LE11 3TU, UK.
†E-mail: S.E.Dann@lboro.ac.uk

Received 31 May 2016; Revised 13 February 2017; Accepted 17 February 2017

1. INTRODUCTION

Humanity's drive to satiate its ever growing energy needs has led to a great surge in research activity in the general area of energy generation and storage. In particular, due to targets enshrined in law in many countries to reduce greenhouse gas emissions in the near future, it is necessary to develop fuels which are capable of delivering energy in a clean and sustainable way [1]. Hydrogen is a very promising candidate fuel as it is carbon-free and has a large chemical energy per unit mass (39.4 kWh kg^{-1}) [2,3]. In addition, the only byproduct of its combustion is water [4]. However, its utility as a fuel for portable and vehicular applications is limited due to its low density (0.0824 g L^{-1} at 298 K) [5], meaning that gaseous hydrogen must be heavily compressed in order for a sufficient quantity to be carried to power devices and vehicles for a sufficiently long period of time to be of practical use [6].

To overcome this problem, in recent years, much interest has been directed at various methods of storing hydrogen in materials, of which chemical hydrogen storage is perhaps the most promising [7–15]. Such materials either release hydrogen upon heating (thermolysis) or by a chemical reaction, usually with water (hydrolysis) [16,17]. The latter, which typically releases hydrogen at temperatures of less than 100 °C, is perhaps the most promising for portable hydrogen storage applications due to its operational convenience. Such an approach is not new; indeed, water hydrolysis was being used on a large scale more than one hundred years ago to generate hydrogen for airships. One of the most important materials used for this purpose was ferrosilicon, an alloy of iron and silicon which generates hydrogen by reacting with hot sodium hydroxide solutions [18–20].

Ferrosilicon alloys are made up of varying mixtures of iron silicides, principally Fe_3Si, Fe_5Si_3, FeSi and $FeSi_2$, and silicon metal [21]. They are produced from

coke, quartz and iron or iron ore in either a blast furnace (for silicon content of up to 15%) or a submerged arc furnace (for silicon content greater than 15%) [22–27]. The mixture of iron silicide phases formed is dependent upon both the proportion of silicon in the alloy, as shown in Table I, and the reaction temperature.

Weaver [20] found that the yield of hydrogen generated from ferrosilicon varied with the silicon content of the ferrosilicon alloy, with a silicon content of <75% giving very low yields of hydrogen. In general, the closer the silicon content to 100%, the higher the obtained yield of hydrogen. This suggests that the presence of elemental silicon in ferrosilicon is crucial for hydrogen generation purposes because elemental silicon is only present in significant quantities in ferrosilicon samples that contain greater than 66.7% silicon by atomic weight (see Table I). Silicon has previously been reported to generate hydrogen by reaction with aqueous sodium hydroxide solutions by many authors according to the following equation: [28–32]

$$Si(cr) + 2\,OH^{-}(aq) + 2\,H_2O(l) - > SiO_2(OH)_2^{2-}(aq) + 2\,H_2(g).$$

In previous work, we estimated the Arrhenius activation energy for the reaction of ferrosilicon 75 with aqueous sodium hydroxide solutions to generate hydrogen [33]. This paper reports a comprehensive study in which we sought to clarify the roles of the elemental silicon and iron–silicon alloy phases in the reaction of the mixed phase material known as ferrosilicon with sodium hydroxide solution to generate hydrogen. In particular, this study aimed to investigate whether iron–silicon alloy phases in ferrosilicon contribute to hydrogen generation or are simply spectator phases. To this end, for the first time, the roles of the elemental silicon and iron disilicide components of ferrosilicon 75 in the release of hydrogen from a commercially available ferrosilicon 75 alloy were investigated by X-ray photoelectron spectroscopy (XPS) and powder X-ray diffraction (PXRD). Comparison reactions with both ferrosilicon 45 (~45 wt.% Si, ~55 wt.% Fe) and $FeSi_2$ were also conducted to investigate their hydrogen generation properties.

2. EXPERIMENTAL

Ferrosilicon 75 (74–77 wt.% Si, 21–24 wt.% Fe), ferrosilicon 45 (~45 wt.% Si, ~55 wt.% Fe) and iron disilicide (20 mesh) were purchased from Castree Kilns and Alfa Aesar, respectively. Sodium hydroxide (reagent grade) and silicon (325 mesh) were purchased from Sigma Aldrich. All chemicals were used as received. To investigate the course of the reaction between ferrosilicon and sodium hydroxide solution, 5 mL of 40 wt.% sodium hydroxide solution was added to a 50-mL round-bottomed flask and left to equilibrate in a water bath for 10 min. To this was then added 1.00 g of ferrosilicon, and the volume of hydrogen evolved was recorded over a 10-min period using the water displacement method [33–35]. In this method, the gas is evolved in a reaction chamber and then transported via a tube to an inverted measuring cylinder filled with water. The open end of the measuring cylinder is immersed in a water reservoir. When gas flows through the tube, water is pushed out of the tube to equalize the pressure of the gas on the inside and outside of the tube. The amount of gas evolved in a given time period can be found by calculating the difference between the starting and finishing level of water in the measuring cylinder. The hydrogen generation reaction was then rapidly quenched by the addition of room temperature distilled water, and the remaining solid isolated by gravity filtration and dried in air. Each reaction was performed in triplicate.

Powder X-ray diffraction (PXRD) data were collected in reflection geometry on a Bruker D8 Advance diffractometer using Cu Kα1 radiation and a LynxEye detector and in transmission geometry on a Bruker D8 Discover diffractometer using Co Kα1 radiation and a Braun linear position sensitive detector. When using the Bruker D8 Advance diffractometer, data were collected over the 2θ range 15–95° with a step size of 0.04° 2θ and a count time of 4.0 s per step, and when using the Bruker D8 Discover diffractometer, data were collected over the 2θ range 15–95° with a step size of 0.007° 2θ and a count time of 1.0 s per step. Phases were identified by comparison to the International Centre for Diffraction Data (ICDD) powder diffraction database (PDF-2 Release 2011, software version: 4.11.3.3, database version: 2.1102). A VG Scientific Escalab Mk I instrument operating with a monochromatic Al Kα X-ray source (1486.6 eV) was used for XPS analysis. The ferrosilicon 75 powders were studied using a Leo 1530 VP field emission gun scanning electron microscope at an accelerating voltage of 5 kV and a working distance of 12 mm. Energy dispersive X-ray spectroscopy was also carried out using the same instrument, with an accelerating voltage of 20 kV and a working distance of 8.5 mm.

Table I. Composition of ferrosilicon alloys of varying silicon content.

Silicon/at.%	Major phases	References
1.9–7.6	α-Fe	[46]
21.3–50	Fe_3Si and FeSi	[46]
50–66.7	FeSi and $FeSi_2$	[47]
66.7+	$FeSi_2$ and Si	[22,36,48,49]

3. RESULTS AND DISCUSSION

3.1. Characterization of ferrosilicon

The phase and surface composition of the ferrosilicon 75 powder used in these experiments was first investigated by PXRD and XPS, respectively. Initially, PXRD patterns were collected in reflection mode using Cu kα1 radiation, but the high background due to iron fluorescence made

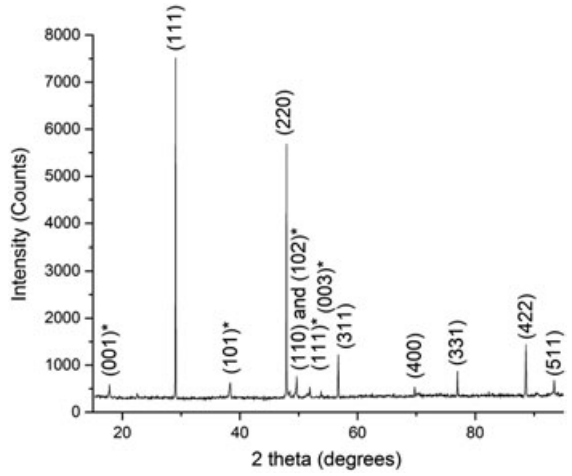

Figure 1. Powder X-ray diffraction (PXRD) pattern for ferrosilicon 75 collected using Cu $K\alpha_1$ radiation in reflection geometry. The (hkl) values for the reflections corresponding to silicon and iron disilicide (β-$FeSi_2$) are labelled (those for iron disilicide are indicated by *)

it difficult to positively identify the lower intensity reflections (Figure 1), and so further XRD patterns were collected in transmission mode with Co $K_{\alpha 1}$ radiation (Figure 2) and compared with the ICDD database. The difference in the background slope between the two samples is due to the use of polymeric tape to mount the sample in transmission instrument. This confirmed that the ferrosilicon 75 powders in this study were formed primarily of Si (cubic, Fd-3m (227), PDF 00-026-1481) and β-$FeSi_2$ (tetragonal, P4/mmm (123), PDF 00-035-0822). Other weak reflections corresponding to minor impurity phases which are commonly observed in commercial ferrosilicon 75 alloys, such as feldspars, quartz, graphite and transition metal oxides such as iron oxide (haematite, magnetite),

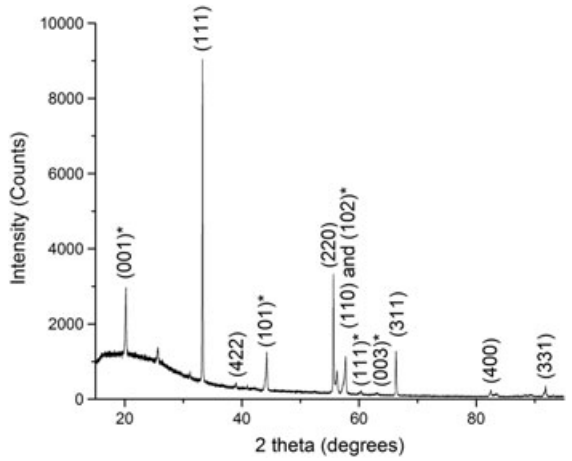

Figure 2. PXRD pattern for ferrosilicon 75 collected using Co $K\alpha_1$ radiation in transmission geometry. The (hkl) values for the reflections corresponding to silicon and iron disilicide (β-$FeSi_2$) are labelled (those for iron disilicide are indicated by *)

were sometimes observed. These are to be expected as ferrosilicon 75 is an industrial grade product made from geologically sourced materials which can vary in composition [36]. Ferrosilicon 45 was also characterized using PXRD (Figure 3) and found to consist primarily of Fe_3Si (cubic, Fm-3m (225), PDF 03-065-0146) as a major phase with minor $FeSi_2$ (tetragonal, P4/mmm (123), PDF 00-035-0822) and α-Fe phases (cubic, Im-3m (229), PDF 03-065-4899). The PXRD analysis furnished no evidence of the presence of a metallic silicon phase in ferrosilicon 45.

Comparator data for the XPS study were collected on single phase silicon and iron silicide. The Si 2p region of the XPS spectra for silicon, iron disilicide and ferrosilicon 75 are shown in Figure 4. All three materials have peaks at 103.1 eV, which corresponds to a surface silicon dioxide layer. The silicon 2p peak is at 99.1 eV, while the silicide 2p peak is at 99.7 eV. In ferrosilicon 75, the peak in the

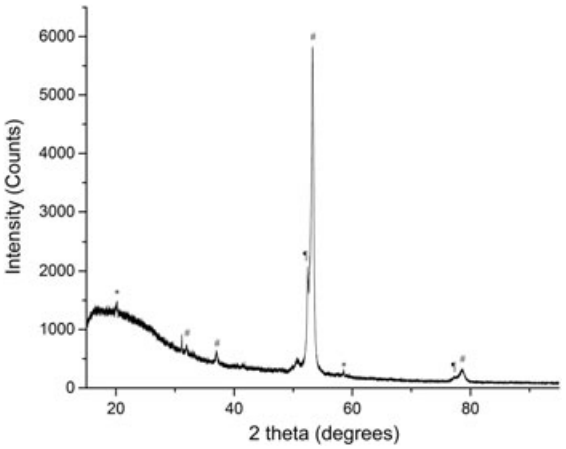

Figure 3. PXRD pattern for ferrosilicon 45 collected using Co $K\alpha_1$ radiation in transmission geometry. The reflections corresponding to Fe_3Si (#), α-Fe (¶) and iron disilicide (*) are indicated

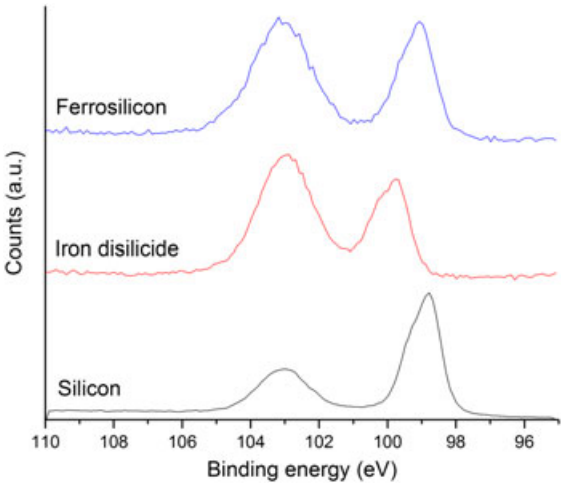

Figure 4. Si 2p region of the X-ray photoelectron spectroscopy (XPS) spectrum obtained for ferrosilicon 75, silicon and iron disilicide

Si(0) region is slightly shifted from that of pure silicon towards that of the silicide and has a shoulder (on the left hand side of the peak in Figure 4). This suggests that this peak is a composite formed predominantly of the silicon 2p peak, with an amount of iron disilicide leading to the shift and the shoulder. The XPS spectra thus indicate that ferrosilicon 75 is coated with a layer of SiO_2, beneath which lies a layer of silicon. The binding energy of the Fe $2p_{3/2}$ peak in the high-resolution XPS scan (Figure 5) of the Fe 2p region matches that which has been previously reported for iron disilicide (707.2 eV) [37]. The atomic composition found by XPS suggests an approximate Si: Fe atomic ratio of ~30:1, indicating that the surface of ferrosilicon 75 is rich in silicon.

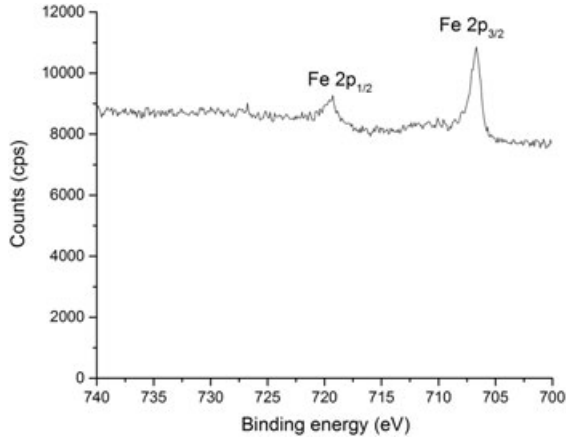

Figure 5. Fe 2p region of the XPS spectrum obtained for ferrosilicon 75

The ferrosilicon 75 powders in this study were used as received and inhomogeneous in particle size, as can be seen from the field emission gun scanning electron microscope image in Figure 6. Ferrosilicon alloys have previously been reported to be inhomogeneous in elemental distribution [38], and the elemental maps obtained by energy dispersive X-ray shown in Figure 7 show that this is also the case for the ferrosilicon 75 used in this study. The ferrosilicon 75 powders consist of regions of silicon and iron disilicide interspersed with small amounts of other phases containing elements such as aluminium. The presence of aluminium also fits with the naturally sourced materials causing low volume impurities such as feldspar type phases (e.g. $NaAlSi_3O_8$). However, despite the inhomogeneity of ferrosilicon 75 at a microscale level, in our previous work, it was found that the volumes of hydrogen evolved from the reaction of 0.75, 1.00, 1.25 and 1.50 g of ferrosilicon 75 with 40 wt.% sodium hydroxide solutions were highly reproducible, suggesting that the average compositions of these masses of ferrosilicon 75 powder were similar [33].

3.2. The roles of silicon and iron disilicide in the hydrogen generation reaction

In previously reported work, to estimate the Arrhenius activation energy for the reaction of ferrosilicon with aqueous sodium hydroxide solutions to generate hydrogen, ferrosilicon 75 (1.0 g) was reacted with 5 mL of 40 wt.% sodium hydroxide solution in a water bath at varying

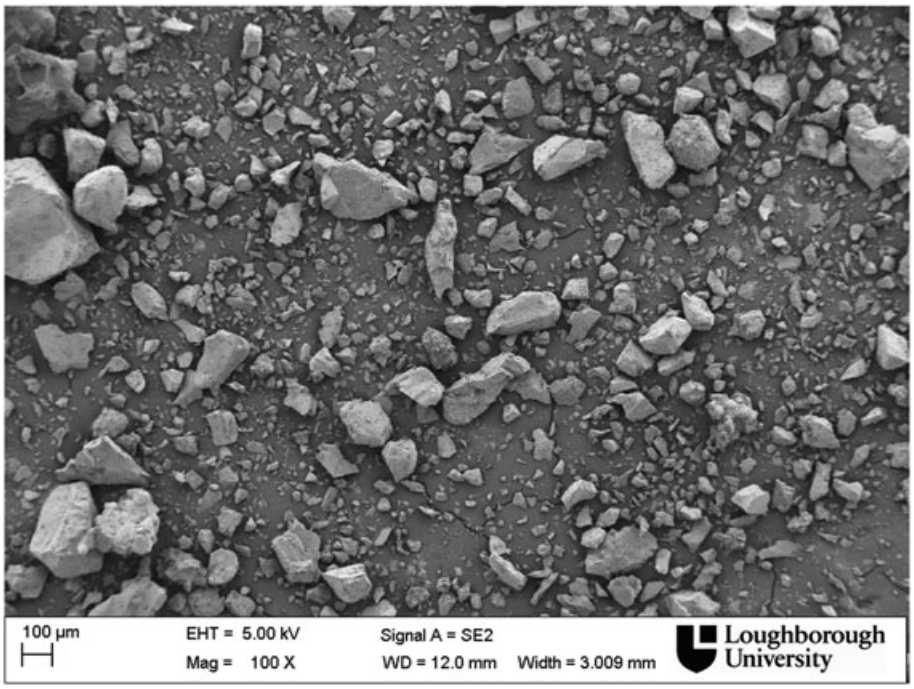

Figure 6. Field emission gun scanning electron microscope (FEG-SEM) image of the ferrosilicon 75 powder used in this study

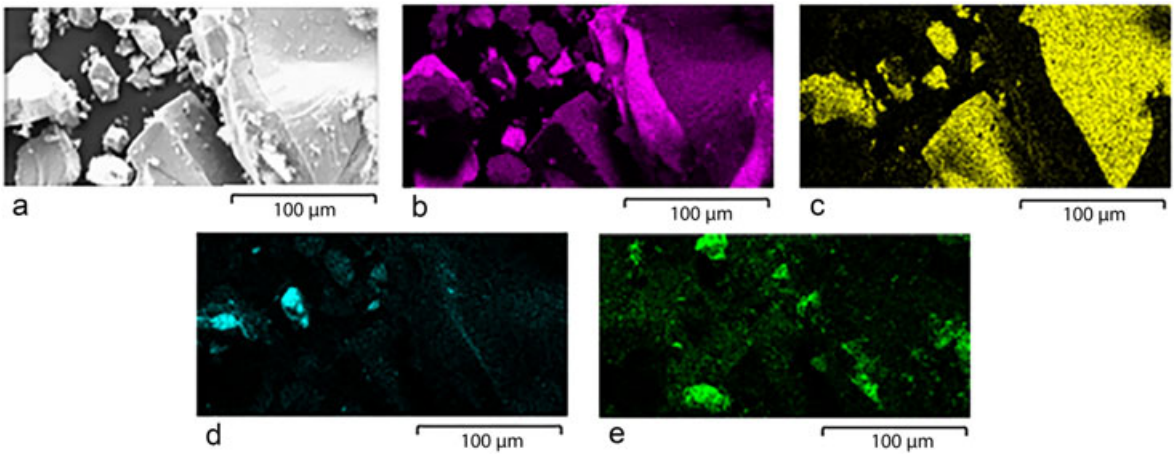

Figure 7. Energy dispersive X-ray (EDX) maps of elemental distributions in the ferrosilicon 75 powder shown in the SEM image (a). Maps are shown for (b) Si, (c) Fe, (d) Al and (e) O

temperatures in the range 331–348 K (57–75 °C) [33]. The volume of hydrogen evolved was measured using the water displacement method. A hydrogen yield of 462.5 mL/g and a maximum hydrogen generation rate of 83 mL/min g were obtained within 10 min at 348 K. In order to investigate the role of the major phases in the hydrogen generation reaction, the reaction was stopped after 10 min by removing the reaction mixture from the water bath and quenching with cold distilled water, and the remaining solid was isolated by gravity filtration and air dried. The hydrogen evolution curves are shown in Figure 8. As described in our previous work [33], the induction period observed before the onset of hydrogen generation is due to the presence of a surface oxide layer which passivates the ferrosilicon 75. The etching of this layer by sodium hydroxide solution is an Arrhenius process, and, thus, the induction period varies exponentially with temperature.

Figure 9 shows that both the total volume of hydrogen evolved in the 10-min period and the mass of ferrosilicon 75 recovered after the 10-min reaction period varied linearly with temperature. In order to elucidate the involvement of silicon and iron disilicide in the hydrogen generation reaction, the recovered ferrosilicon 75 powders were analysed by PXRD and XPS.

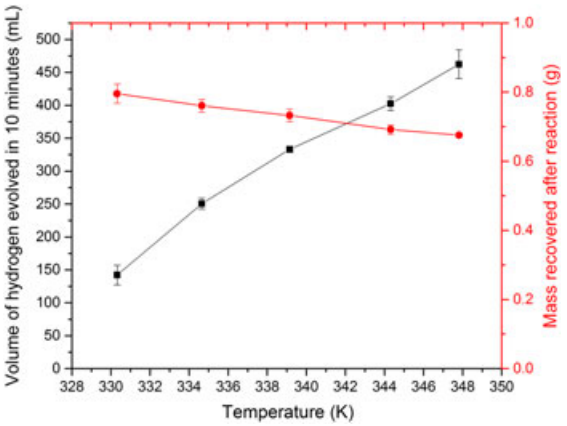

Figure 9. A plot showing the effect of reaction temperature on the mass of solid recovered (red circles) and volume of hydrogen generated after 10 min of reaction (black squares) with 40 wt.% sodium hydroxide solution. The error bars show one standard deviation

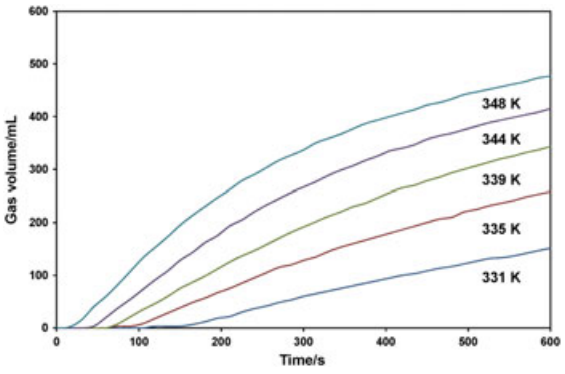

Figure 8. Hydrogen generation curves at 331 K (blue), 335 K (red), 339 K (green), 344 K (purple) and 348 K (turquoise) from the reaction of 1.00 g of ferrosilicon 75 with 5 mL of a 40 wt.% sodium hydroxide solution. From Ref. 33

It is clear from the PXRD patterns shown in Figure 10 that the relative intensities of the reflections corresponding to the silicon (111) and (220) planes decrease with respect to those corresponding to the iron disilicide reflections as the temperature of the reaction (and volume of hydrogen obtained from the reaction) increases. While intensity in diffraction is not directly correlated with quantity due to the requirement for the phases to be crystalline, the implication is that the silicon phase is affected during the reaction in a way that the iron silicide is not. This would strongly suggest that the vast majority of hydrogen is

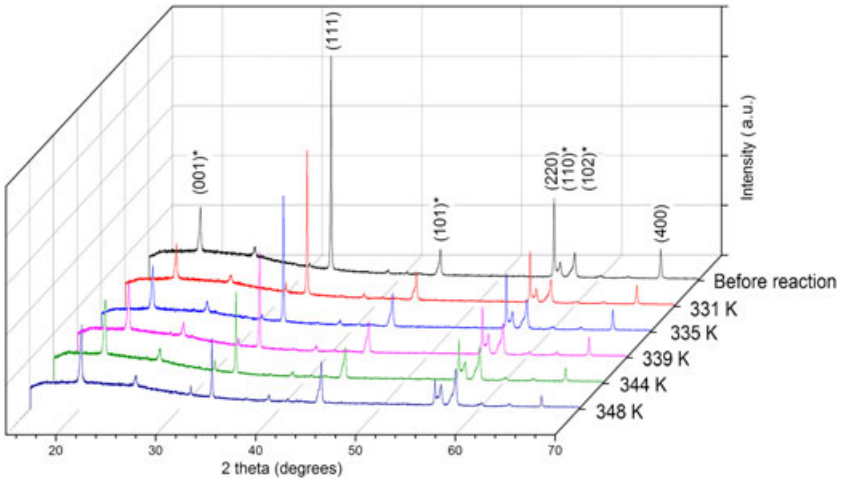

Figure 10. PXRD patterns for recovered ferrosilicon powders collected using Co Kα radiation in transmission geometry. The (hkl) values for the reflections corresponding to silicon and iron disilicide (β-$FeSi_2$) are labelled (those for iron disilicide are indicated by *)

generated due to the reaction and likely consumption of the silicon phase.

The XPS data gives a further insight into the process of the hydrogen generation reaction. The Si 2p region of the ferrosilicon 75 powders recovered after reaction for 10 min in water baths at differing temperatures is shown in Figure 11. As detailed in Section 3.1, the peaks in Si 2p spectrum for ferrosilicon 75 correspond to silicon oxide (103.1 eV) and a composite peak formed of the responses

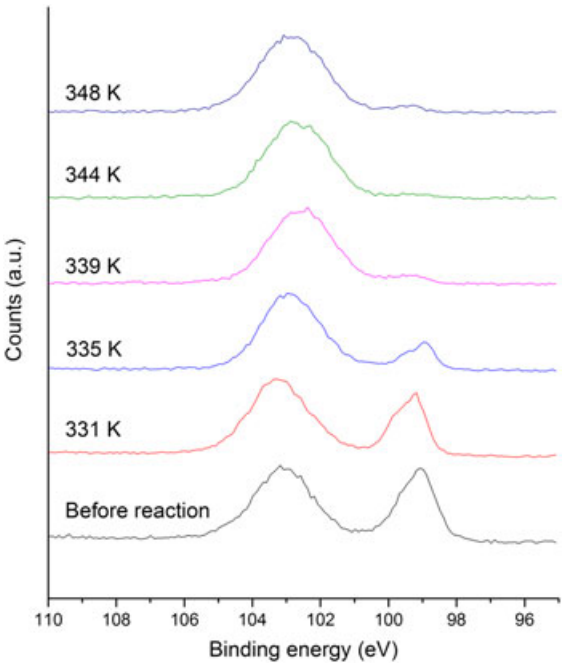

Figure 11. XPS spectra showing the Si 2p region of ferrosilicon 75 samples recovered at 10-min reaction time in a water bath at the temperatures indicated in the figure

for iron disilicide and silicon. As the volume of hydrogen generated increases with reaction temperature, the peak corresponding to iron disilicide and silicon gradually reduces in size until it is barely visible in the samples reacted at above 344 K. There is a gradual shift towards a lower binding energy of the peak initially assigned to silicon dioxide as the temperature, and thus volume of hydrogen evolved is increased. It is known that sodium silicate shows a peak at 102.2 eV [39], and thus it is postulated that the shifted peak is formed of the signals from silicon dioxide and sodium silicate. Sodium silicate has been reported as a by-product of the reaction between silicon and sodium hydroxide solution (to form hydrogen), and so this complements the PXRD data already detailed [40–42]. Indeed, this build-up of sodium silicate at the surface of the material could also be the cause of the gradual reduction in reaction rate over time observed at higher temperatures, as it would impede access of the solution to the silicon phase due to the viscous nature of colloidal silicate solutions cf. waterglass [43].

In addition, the O 1s region (Figure 12) of the XPS spectra provides evidence for the presence of a silicate species alongside silicon dioxide on the surface of the isolated ferrosilicon 75 powders. It has been reported that sodium silicate has peaks at 530.5 and 532.6 eV [44], while silicon dioxide has a peak at 532.3 eV [45]. The peaks observed in the ferrosilicon 75 isolated from the reactions at 335 K and above are clearly formed of at least one pair of overlapping signals, and a composite peak generated from those known for sodium silicate and silicon dioxide would be expected to be observed in this area of the spectrum.

The Fe 2p regions of the XPS spectra for the same samples are shown in Figure 13. The small peaks at ~712 eV are suggestive of the $2p_{3/2}$ signal for Fe_2O_3, but perhaps the clearest message from this data is that there remains very little iron at the surface of the powders after the hydrogen generation reactions.

DOI: 10.1002/er

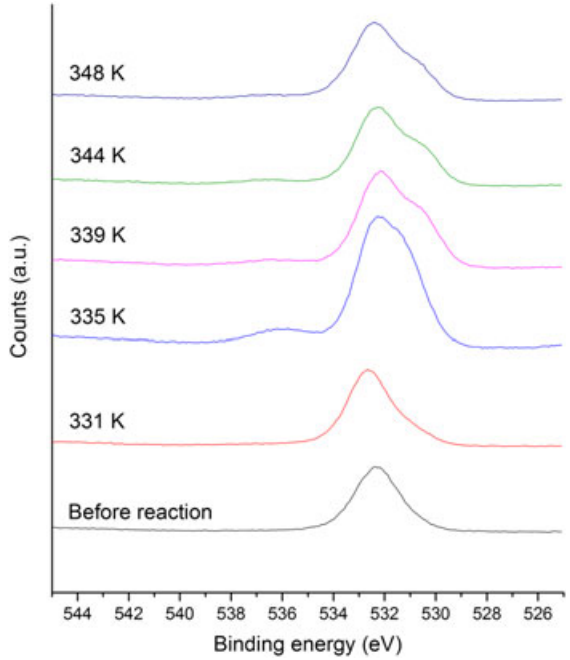

Figure 12. XPS spectra showing the O 1s region of ferrosilicon 75 samples recovered at 10-min reaction time in a water bath at the temperatures indicated in the figure

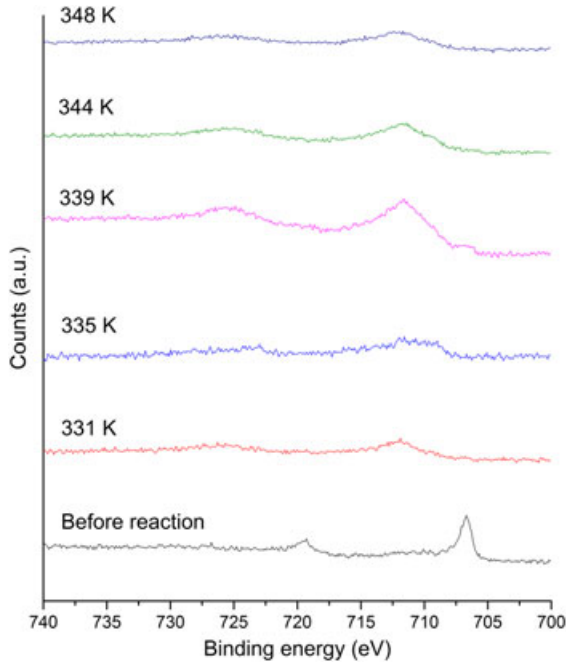

Figure 13. XPS spectra showing the Fe 2p region of ferrosilicon 75 samples recovered at 10-min reaction time in a water bath at the temperatures indicated in the figure

The analysis of the ferrosilicon 75 powders isolated at different stages of reaction thus indicates that the generation of hydrogen by the reaction of ferrosilicon 75 with sodium hydroxide solutions is entirely due to the reaction of silicon. To prove this hypothesis, hydrogen evolution experiments were also performed on a different ferrosilicon alloy (ferrosilicon 45, containing predominantly Fe_3Si, $FeSi_2$ and Fe) and on iron disilicide itself. Ferrosilicon 45 did not produce any hydrogen under these reaction conditions, in keeping with our hypothesis that the metallic silicon phase is critical for hydrogen generation. Furthermore, the pure iron disilicide produced no measurable hydrogen output using the same experimental setup, indicating that iron disilicide does not produce any hydrogen over a useful timescale. We hypothesize that the role of iron disilicide is simply that of a 'blocker', slowing the rate of the reaction between hydroxide and silicon to give a lower but more sustained rate of hydrogen generation than that which could be obtained from silicon powder. The specific idea of the blocker is that the ferrosilicon 75 samples are mixtures of silicon and iron disilicide. Ferrosilicon 75 itself is formed in a blast furnace at very high temperature meaning that the particles are rarely mixtures of $FeSi_2$ and Si particles on their own but conglomerated particles of both $FeSi_2$ and Si together. These conglomerates can be arranged in different ways, but if the $FeSi_2$ is on the outside and the Si is in the middle and the former does not react with either air or sodium hydroxide solution, it will effectively block the silicon from reaction. This is especially advantageous for stationary applications where a sustained, steady flow of hydrogen, over a long period of time, rather than a sudden surge, is required and could also be useful for portable applications if the activation energy of the hydrogen generating reaction could be sufficiently lowered and the induction time reduced. This would also serve to explain the observation of Weaver [20] that high silicon content ferrosilicon alloy is required for hydrogen generation, as it is only these alloys which contain a metallic silicon phase.

4. CONCLUSIONS

These experimental data strongly suggest that the generation of hydrogen from ferrosilicon 75 is due to the reaction of silicon with sodium hydroxide solution. The finding that the reactions of iron disilicide alone and ferrosilicon 45 with sodium hydroxide solution under similar conditions did not lead to hydrogen generation offers further confirmation of the essential nature of the metallic silicon phase for hydrogen generation. Iron disilicide does not appear to play a direct role in the reaction, but instead we hypothesize that it acts as a 'blocker' which slows the rate of hydrogen generation from silicon, giving a steady, long lived supply of hydrogen suited to stationary applications. In addition, due to its widespread use in the steel industry, ferrosilicon 75 is available by the tonne at a lower cost than the majority of chemical hydrogen storage materials, making it an ideal material for large-scale hydrogen generation applications. A hydrogen yield of 462.5 mL/g and a maximum hydrogen generation rate of 83 mL/min g were obtained within 10 min of reaction with 40 wt.% NaOH at 348 K.

ACKNOWLEDGEMENTS

The authors would like to thank the EPSRC and Intelligent Energy for funding this project. P.B. would also like to thank the SCI for the award of a Messel Scholarship. The authors acknowledge use of the facilities and the assistance of Pat Cropper and Dr Keith Yendall in the Loughborough Materials Characterisation Centre.

REFERENCES

1. Dincer I, Acar CA. Review on clean energy solutions for better sustainability. *International Journal of Energy Research* 2015; **39**:585–606.
2. Acar C, Dincer I. Impact assessment and efficiency evaluation of hydrogen production methods. *International Journal of Energy Research* 2015; **39**:1757–1768.
3. Zuttel A, Borgschulte A, Schlapbach L (Eds). *Hydrogen as a Future Energy Carrier*. Wiley-VCH: Weinheim, 2008.
4. Schlapbach L, Züttel A. Hydrogen-storage materials for mobile applications. *Nature* 2001; **414**:353–358.
5. Haynes WM (Ed). *CRC Handbook of Chemistry and Physics, 95th Edition, 2014–15*. CRC Press: Boca Raton, 2014.
6. Tsuchiya H. Innovative renewable energy solutions for hydrogen vehicles. *International Journal of Energy Research* 2008; **32**:427–435.
7. David WIF. Effective hydrogen storage: a strategic chemistry challenge. *Faraday Discussions* 2011; **151**:399–414.
8. Eberle U, Felderhoff M, Schüth F. Chemical and physical solutions for hydrogen storage. *Angewandte Chemie International Edition in English* 2009; **48**:6608–6630.
9. Jena P. Materials for hydrogen storage: past, present, and future. *Journal of Physical Chemistry Letters* 2011; **2**:206–211.
10. Yang J, Sudik A, Wolverton C, Siegel DJ. High capacity hydrogen storage materials : attributes for automotive applications and techniques for materials discovery. *Chemical Society Reviews* 2010; **39**:656–675.
11. Weidenthaler C, Felderhoff M. Solid-state hydrogen storage for mobile applications: quo vadis? *Energy and Environmental Science* 2011; **4**:2495–2502.
12. Sakintuna B, Lamaridarkrim F, Hirscher M. Metal hydride materials for solid hydrogen storage: a review. *International Journal of Hydrogen Energy* 2007; **32**:1121–1140.
13. Orimo SI, Nakamori Y, Eliseo JR, Züttel A, Jensen CM. Complex hydrides for hydrogen storage. *Chemistry Review* 2007; **107**:4111–4132.
14. Nielsen TK, Besenbacher F, Jensen TR. Nanoconfined hydrides for energy storage. *Nanoscale* 2011; **3**:2086–2098.
15. Brack P, Dann SE, Wijayantha KGU. Heterogeneous and homogenous catalysts for hydrogen generation by hydrolysis of aqueous sodium borohydride ($NaBH_4$) solutions. *Energy Science & Engineering* 2015; **3**:174–188.
16. Marrero-Alfonso EY, Beaird AM, Davis TA, Matthews MA. Hydrogen generation from chemical hydrides. *Industrial and Engineering Chemistry Research* 2009; **48**:3703–3712.
17. Durbin DJ, Malardier-Jugroot C. Review of hydrogen storage techniques for on board vehicle applications. *International Journal of Hydrogen Energy* 2013; **38**:14595–14617.
18. Taylor HS. *Industrial Hydrogen*. The Chemical Catalog Company, Inc.: New York, USA, 1921.
19. Teed PL. *The Chemistry and Manufacture of Hydrogen*. Edward Arnold: London, 1919.
20. Weaver ER. The generation of hydrogen by the reaction between ferrosilicon and a solution of sodium hydroxide. *Journal of Industrial and Engineering Chemistry* 1920; **12**:232–240.
21. Dahal N, Chikan V. Phase-controlled synthesis of iron silicide (Fe 3 Si and FeSi 2) nanoparticles in solution. *Chemistry of Materials* 2010; **22**:2892–2897.
22. Ingason HT, Jonsson GR. Control of the silicon ratio in ferrosilicon production. *Control Engineering Practice* 1998; **6**:1015–1020.
23. Hauksdottir AS, Gestsson A, Vesteinsson A. Submerged-arc ferrosilicon furnace simulator : validation for different furnaces and operating ranges. *Control Engineering Practice* 1998; **6**:1035–1042.
24. Hauksdottir AS, Gestsson A, Vesteinsson A. Current control of a three-phase submerged arc ferrosilicon furnace. *Control Engineering Practice* 2002; **10**:457–463.
25. Buø TV, Gray RJ, Patalsky RM. Reactivity and petrography of cokes for ferrosilicon and silicon production. *International Journal of Coal Geology* 2000; **43**:243–256.
26. Farzana R, Rajarao R, Sahajwalla V. Synthesis of ferrosilicon alloy using waste glass and plastic. *Materials Letters* 2014; **116**:101–103.
27. Farzana R, Rajarao R, Sahajwalla V. Characteristics of waste automotive glasses as silica resource in ferrosilicon synthesis. *Waste Management & Research* 2016; **34**:113–121.
28. Brack P, Dann SE, Wijayantha KGU, Adcock P, Foster S. An assessment of the viability of hydrogen generation from the reaction of silicon powder and sodium hydroxide solution for portable applications. *International Journal of Energy Research* 2017; **41**(2):220–228.

29. Seidel H, Csepregi L, Heuberger A, Baumgartel H. Anisotropic etching of crystalline silicon in alkaline solutions. *Journal of the Electrochemical Society* 1990; **137**:3612–3626.
30. Shah IA, Koekkoek AJJ, van Enckevort WJP, Vlieg E. Influence of additives on alkaline etching of silicon(111). *Crystal Growth and Design* 2009; **9**:4315–4323.
31. Kao TL, Huang WH, Tuan HY. Kerf loss silicon as a cost-effective, high-efficiency, and convenient energy carrier: additive-mediated rapid hydrogen production and integrated systems for electricity generation and hydrogen storage. *Journal of Materials Chemistry A* 2016; **4**:12921–12928.
32. Palik ED, Bermudez VM, Glembocki OJ. Ellipsometric study of orientation-dependent etching of silicon in aqueous KOH. *Journal of the Electrochemical Society* 1985; **132**:871–884.
33. Brack P, Dann SE, Wijayantha KGU, Adcock P, Foster S. An old solution to a New problem? Hydrogen generation by the reaction of ferrosilicon with aqueous sodium hydroxide solutions. *Energy Science & Engineering* 2015; **3**:535–540.
34. Shang Y, Chen R, Jiang G. Kinetic study of $NaBH_4$ hydrolysis over carbon-supported ruthenium. *International Journal of Hydrogen Energy* 2008; **33**:6719–6726.
35. Brack P, Dann SE, Wijayantha KGU, Adcock P, Foster S. A simple, low-cost, and robust system to measure the volume of hydrogen evolved by chemical reactions with aqueous solutions. *Journal of Visualized Experiments* 2016; **114**:e54383.
36. Margarido F, Figueiredo MO. CAALSIFER: a quaternary Fe–Al–Si–Ca phase isotypic with a-leboite ($Fe_{1-x}Si_2$). *Materials Science and Engineering A* 1988; **104**:249–254.
37. Ohtsu N, Oku M, Satoh K, Wagatsuma K. Dependence of core-level XPS spectra on iron silicide phase. *Applied Surface Science* 2013; **264**:219–224.
38. Zakharov RG, Petrova SA, Zhdanov AV, Zhuchkov VI. Effect of the structure of ferrosilicon on its desintegration. *Russian Metallurgy* 2014; **1**:8–13.
39. Mekki A, Holland D, McConville CF, Salim M. An XPS study of iron sodium silicate glass surfaces. *Journal of Non-Crystalline Solids* 1996; **208**:267–276.
40. Palik ED, Gray HF, Klein PB. A Raman study of etching silicon in aqueous KOH. *Journal of the Electrochemical Society* 1983; **130**:956–959.
41. Allongue P, Costa-Kieling V, Gerishcher H. Etching of silicon in NaOH solutions. *Journal of the Electrochemical Society* 1993; **140**:1018–1026.
42. Glembocki OJ, Palik ED, Deguel GR, Kendall DL. Hydration model for the molarity dependence of the etch rate of Si in aqueous alkali hydroxides. *Journal of the Electrochemical Society* 1991; **138**:1055–1063.
43. Garcia S, Bao H, Hines M. Etchant anisotropy controls the step bunching instability in KOH etching of silicon. *Physical Review Letters* 2004; **93**:166102.
44. Sprenger D, Bach H, Meisel W, Gi P. XPS study of leached glass surfaces. *Journal of Non-Crystalline Solids* 1990; **126**:111–129.
45. Pitts JR, Thomas TM, Czanderna AW. XPS and ISS of submonolayer coverage of Ag on SiO_2*. *Applied Surface Science* 1986; **26**:107–120.
46. Wolff U, Schneider F, Mummert K, Schultz L. Stability and electrochemical properties of passive layers on Fe–Si alloys. *Corrosion* 2000; **56**:1195–1201.
47. Halmann M, Frei A, Steinfeld A. Magnesium production by the pidgeon process involving dolomite calcination and MgO silicothermic reduction: thermodynamic and environmental analyses. *Industrial and Engineering Chemistry Research* 2008; **47**:2146–2154.
48. Margarido F, Bastos MH, Figueiredo MO, Martins JP. The structural effect on the kinetics of acid leaching refining of Fe–Si alloys. *Materials Chemistry and Physics* 1994; **38**:342–347.
49. Wang Y, Cheng L, Guan J, Zhang L. Effect of dilution and additive on direct nitridation of ferrosilicon. *Journal of the European Ceramic Society* 2014; **34**:1115–1122.